frontiers in Earth Science

ORIGINAL RESEARCH
published: 17 September 2021
doi: 10.3389/feart.2021.758619

Interdecadal Linkage Between the Winter Northern Hemisphere Climate and Arctic Sea Ice of Diverse Location and Seasonality

Xulong He[1], *Ruonan Zhang*[1,2,3]*, *Shuoyi Ding*[1] *and Zhiyan Zuo*[1]

[1]*Department of Atmospheric and Oceanic Sciences, Institute of Atmospheric Sciences, Fudan University, Shanghai, China,* [2]*Shanghai Qi Zhi Institute, Shanghai, China,* [3]*Innovation Center of Ocean and Atmosphere System, Zhuhai Fudan Innovation Research Institute, Zhuhai, China*

During the past few decades, Arctic sea-ice has declined rapidly in both autumn and winter, which is likely to link extreme weather and climate events across the Northern Hemisphere midlatitudes. Here, we use reanalysis data to investigate the possible linkage between mid–high-latitude atmospheric circulation and Arctic sea-ice loss in different geographical locations and seasons and associated impacts on wintertime climate on interdecadal timescales. Four critical sea-ice subregions are analyzed in this study—namely, the Pan-Arctic, Barents–Kara–Laptev Seas (BKL), East Siberia–Chukchi–Beaufort Seas (EsCB), and Bering Sea (Ber). Results suggest that interdecadal reduction of autumn sea-ice, irrespective of geographical location, is dynamically associated with the negative phase of the North Atlantic Oscillation (NAO) in the subsequent winter *via* stratospheric pathways. Specifically, autumn sea-ice loss appears to cause a weakened stratospheric polar vortex that propagates to the troposphere in the ensuing months, leading to lower surface air temperature and a deficit in precipitation over Siberia and northeastern North America. Meanwhile, an anomalous cyclone over Europe favors excessive precipitation over southern Europe. For wintertime sea-ice loss in the Pan-Arctic and BKL, a weak positive NAO phase, with a dipole pressure pattern over Greenland–northeastern North America and North Atlantic, and a shrunken Siberian high over Eurasia are observed over mid–high-latitudes. The former results in excessive precipitation over northwestern and southeastern North America, whilst the latter leads to less precipitation and mild winter over Siberia. In contrast, Ber sea-ice loss is associated with a circumglobal wave train downstream of the Bering Sea, leading to extensive warming over Eurasia. The anomalous dipole cyclone and anticyclone over the Bering Sea transport more Pacific and Arctic water vapor to North America, and the anomalous cyclone over the Barents Sea results in abundant precipitation in Siberia. Such midlatitude anomaly is dynamically linked to winter sea-ice loss, mainly through tropospheric rather than stratospheric pathways. These results have important implications for future seasonal and interdecadal forecasts in the context of ongoing sea-ice decline.

Keywords: interdecadal linkage, sea ice, midlatitudes coldness, precipitation, water vapor transport

OPEN ACCESS

Edited by:
Xander Wang,
University of Prince Edward Island, Canada

Reviewed by:
Shangfeng Chen,
Institute of Atmospheric Physics (CAS), China
Sai Wang,
Chinese Academy of Meteorological Sciences, China

***Correspondence:**
Ruonan Zhang
rn_zhang@fudan.edu.cn

Specialty section:
This article was submitted to Interdisciplinary Climate Studies, a section of the journal Frontiers in Earth Science

Received: *14 August 2021*
Accepted: *01 September 2021*
Published: *17 September 2021*

Citation:
He X, Zhang R, Ding S and Zuo Z (2021) Interdecadal Linkage Between the Winter Northern Hemisphere Climate and Arctic Sea Ice of Diverse Location and Seasonality. Front. Earth Sci. 9:758619. doi: 10.3389/feart.2021.758619

INTRODUCTION

In recent decades, the midlatitudes of the Northern Hemisphere have experienced more frequent cold winters and extreme weather events (Wu et al., 2011; Cohen et al., 2014; Li et al., 2015; Cohen et al., 2020; Wang et al., 2021). For instance, Japan suffered an extreme snowstorm in December 2005, and China suffered persistent cold and freezing rain events in January–February 2008 (WMO Regional Climate Centres 2012); and extreme cold conditions and heavy snowfall attacked North America in two consecutive winters (2013/14 and 2014/15), during which the Great Lakes were almost completely frozen for the first time in the previous 35 years and Boston experienced record-breaking snowfall reaching 2.7 m (Van Oldenborgh et al., 2015).

A range of mechanisms have been proposed for the frequent occurrence of extreme cold and snowy climates during the past 2 decades. Some studies have attributed natural variation as the primary cause of Eurasian cooling (Trenberth, 1999; Sun et al., 2016; Song et al., 2016; Screen, 2017B); whereas, in contrast, others have suggested that the increase in cold temperature events has been affected by the so-called Arctic Amplification and associated sea-ice loss (Francis and Vavrus, 2012; Mori et al., 2014, 2019; Takaya and Nakamura, 2015; Zhang et al., 2018; Zhang and Francis, 2020; Zhang et al., 2021). For instance, Wu et al. (2017) investigated a cold event that occurred in East Asia during January–February 2012 and its possible association with Arctic sea-ice loss. They found that weakening of the Aleutian low and rapid strengthening of the Siberian high, concurrent with a polar blocking high aloft, were crucial precursors for cold-air outbreaks from the Arctic. In addition to extreme temperature events, Arctic sea-ice loss further affects wintertime precipitation in northern midlatitudes. Large-scale atmospheric circulation and moisture transport are decisive for this precipitation *via* storm-scale moisture convergence (Ma et al., 2012; Sun and Wang, 2012). Using an atmospheric model, Li and Wang (2012) indicated that a negative phase of the North Atlantic Oscillation (NAO) in response to Kara–Laptev sea-ice loss in autumn acts as an atmospheric ridge over Eurasia that is favorable for moisture transport to East Asia. Liu et al. (2016) reported that the reduction of autumn sea-ice across the Arctic Ocean is accompanied by dry conditions over central China and wet conditions over South China and North China in early winter, *via* two wave-train structures.

There are two main pathways responsible for these Arctic–midlatitude linkages. First is the stratospheric pathway through which Arctic sea-ice loss causes a weakened stratospheric polar vortex in the ensuing months and has lagging effects on midlatitude climate in both winter and the subsequent spring (Mori et al., 2014; Chen and Wu, 2018; Mori et al., 2019). Second is the tropospheric pathway, in which the melting sea-ice decreases polar-to-tropics temperature gradients, which results in meandering tropospheric flow and more extreme weathers events in the midlatitudes (Nakamura et al., 2014; Sun et al., 2015; Nakamura et al., 2016). Another critical issue is the geographical location of sea-ice loss, which has distinct impacts on the midlatitude climate in both modeling and observational studies (Screen, 2017A). Specifically, rapid sea-ice loss in the Barents–Kara–Laptev (BKL) seas has tremendous impacts on the Eurasian climate (Honda et al., 2009), while in the East Siberian–Chukchi–Beaufort (EsCB) seas it has substantial implications for the climate over North America (Kug et al., 2015).

However, most previous studies have tended to focus on sea-ice change in the winter season or year-round and on interannual timescales, with limited attention having been paid to autumn and interdecadal timescales. Although recent studies argued there is diverse Eurasian temperature and precipitation responses to BKL sea-ice loss in autumn (Li and Wang, 2012; Ding et al., 2020; Zhang and Screen, 2021), their focus was on the interannual rather than interdecadal timescale. Chen and Wu (2018) and Ding and Wu (2021) explored how autumn EsCB sea-ice loss can influence spring Eurasian temperature. However, the impact on wintertime temperature and precipitation has not been thoroughly examined, particularly on interdecadal timescales.

This study aims to address two questions: 1) How does Arctic sea-ice loss in different seasons and at different locations contribute to the wintertime atmospheric circulation anomalies and associated impact on temperature and precipitation? 2) What is the Arctic-midlatitude linkage on interdecadal timescales? More specifically, this paper investigates the interdecadal linkage between Northern Hemisphere temperature and precipitation and sea-ice change in diverse regions and seasons. The underlying physical mechanisms of these linkages are thoroughly investigated *via* tropospheric and stratospheric pathways. Before we investigate the interdecadal linkage, the total variation (i.e., the sum of interannual and interdecadal variations) of sea-ice and its association with wintertime climate is primarily analyzed as a comparison.

Data and Methods

The datasets employed in this research are: 1) the National Centers for Environmental Prediction atmospheric reanalysis with a resolution of 2.58° × 2.58° (Kalnay et al., 1996), including sea level pressure (SLP), surface air temperature (SAT), horizontal wind, specific humidity, and geopotential height; 2) the monthly sea-ice concentration (SIC) from the Met Office Hadley Center with a 1° × 1° longitude/latitude resolution (Rayner et al., 2003); and 3) the enhanced monthly mean precipitation from the Climate Prediction Center Merged Analysis of Precipitation with a resolution of 2.5° × 2.5° (Xie and Arkin, 1997). For interdecadal study, the 1959–2020 period is analyzed in the present study. Regression and correlation analysis are employed in this study, and the two-tailed Student's *t*-test is applied to examine the statistical significance of the regression and correlation coefficients.

Based on topographical features (e.g., islands, straits) and conventional nomenclature, sea-ice in the Atlantic and Pacific sectors is analyzed in the present study. Specifically, we set the area-averaged SIC north of 60°N as belonging to the Pan-Arctic. Likewise, we define BKL as the (70°–80°N, 30°–135°E)-averaged SIC to represent Atlantic sea-ice index. In the Pacific sector, autumn sea-ice is mainly located in the EsCB region during September–October, and large variance of winter

(December–February) sea-ice exists in the Bering Sea (Ber) region. The reason why we choose September–October EsCB for autumn analysis is that the melting of sea-ice in EsCB is limited to occurring in September and October, which has great influence on stratospheric processes, whilst subtle sea-ice loss occurs in other months (Chen and Wu, 2018; Ding et al., 2021). Therefore, we define EsCB as the (70.5°–82.5°N, 135°E–60.5°W)-averaged SO SIC and Ber as the (55°–68°N, 165°E–125°W)-averaged DJF SIC to represent Pacific sea-ice indices. Linear trends are removed from the SIC indices prior to carrying out the analysis. In general, this paper emphasizes on autumn sea-ice in Pan-Arctic, BKL and EsCB regions and winter sea-ice in Pan-Arctic, BKL and Ber regions.

To investigate the interdecadal variation of sea-ice, we use power spectrum method to figure out the periodism of Arctic sea-ice indices in diverse regions. Three main periods are identified for autumn and winter sea-ice, which are 2-year, 10-year, and 20-year (figure not shown). Therefore, since our focus is the interdecadal timescale, a 9-year low-pass Butterworth filter is applied to all variables to derive the interdecadal component. The algorithm of the Butterworth low-pass filter (Selesnick and Burrus, 1998) can be expressed by the following formula of the amplitude squared to the frequency:

$$|H(\omega)|^2 = \frac{1}{1+\left(\frac{\omega}{\omega_e}\right)^{2n}} = \frac{1}{1+e^2\left(\frac{\omega}{\omega_p}\right)^{2n}}$$

where n is the filter order (as n increases, the smoother the curve will be), ω_e is the cut-off frequency, and ω_p is the pass-band edge frequency. For example, if we extract decadal components from the original sequence, our sampling frequency is 1 year, and the decadal cycle is 9 years. That is, the frequency is 1/9, and then the end frequency is $\omega_e = 2 \times 1/9 \approx 0.222$.

Besides, the low-pass filtered variables will have strong persistence or high autocorrelation. Therefore, the effective number of degree of freedom of the significance test (i.e., the t-test) needs to be replaced with n/T when calculating the regression and correlation coefficients. The formulae are as follows (Davis, 1976):

$$T = \sum_{j=-\infty}^{\infty} R_{xx}(j) R_{yy}(j),$$

$$R_{xx}(j) = \frac{1}{n-j} \sum_{t=1}^{n-j} x_t^* x_{t+j}^*,$$

$$R_{yy}(j) = \frac{1}{n-j} \sum_{t=1}^{n-j} y_t^* y_{t+j}^*,$$

where R_{xx} and R_{yy} are the autocorrelation coefficients of x and y, respectively; n is the sample number; j is the lag time, usually set as $n/2$; and an asterisk (*) represents normalization.

RESULTS

Interdecadal Variations in Arctic Sea Ice

Arctic sea-ice change has profound impacts on the wintertime climate of the Northern Hemisphere (Cohen et al., 2014; Cohen et al., 2020). Moreover, there is emerging evidence that the geographical location of sea-ice loss is critically important in determining the large-scale atmospheric circulation anomalies and associated impacts on the midlatitudes (Screen, 2017A). Besides, there are diverse winter circulation responses to sea-ice loss in different seasons (Zhang and Screen, 2021). **Figure 1** displays the variations in Arctic SIC in the different regions and seasons. In general, the SIC indices show substantial variations on interannual and interdecadal timescales. The interannual component of SIC indices explained roughly 52.1–78.9% of the total variance, while the interdecadal component explained 21.1–47.9% (**Table 1**). This result indicates that the interdecadal changes in SIC indices are of great importance, in addition to the interannual variability, in the total variations. We find Arctic SIC variations in autumn and winter show particularly high coherence. For instance, for the Pan-Arctic, BKL and Ber, the correlation coefficients between the autumn and winter SIC indices are 0.51, 0.42, and 0.37 respectively, with the statistical significance exceeding the 95% confidence level (**Table 2**). These high correlation coefficients indicate that a large part of the autumn sea-ice change tends to persist until winter. However, for EsCB, the autumn–winter correlation is only 0.26, consistent with the finding of Ding et al. (2021) that the melting of sea-ice in EsCB in September–October doesn't persistent into the following winter.

Such seasonal footprint characteristics in the Pan-Arctic, BKL, and Ber are also seen in the spatial pattern of correlation coefficients (**Figure 2**). When there is more (less) Pan-Arctic SIC in autumn, positive (negative) anomalies of sea-ice are located over the northern BKL and the EScB; however, in the following winter, the highly correlated region shrinks to Eurasian coastal regions, particularly over the Laptev Sea (**Figures 2A,D**). It is interesting to note that the regions of significant Pan-Arctic SIC anomalies cover the BKL and EsCB regions. That is why the correlation coefficients between the Pan-Arctic and BKL and EsCB in autumn reach 0.74 and 0.70, respectively. For BKL and EsCB, positive SIC correlations are limited to the defined region (**Figures 2B,C**), but only the southern part lasts to winter (**Figures 2E,F**).

In comparison, the wintertime sea-ice in association with winter SIC indices differs from those with autumn SIC indices. When the winter Pan-Arctic index is above average, positive SIC anomalies are located over the Atlantic sector (northern Barents–Kara–Greenland seas) and Pacific sector (Chukchi–Bering seas), which also covers the BKL and Ber regions (**Figures 2G–I**). Nevertheless, the correlation coefficients between the winter Pan-Arctic and BKL and Ber SIC indices are 0.83 and 0.30, respectively, indicating that the winter BKL makes major contributions to the variations in Pan-Arctic SIC.

Sea-ice indices in different regions and seasons show apparent interdecadal variations, which explain approximately half of the total variations. The Pan-Arctic index shows similar interdecadal changes to those of BKL in both autumn and winter, with negative phases during 1980–1990 and during 2005–2020, and a positive phase during 1990–2000. The two indices are also

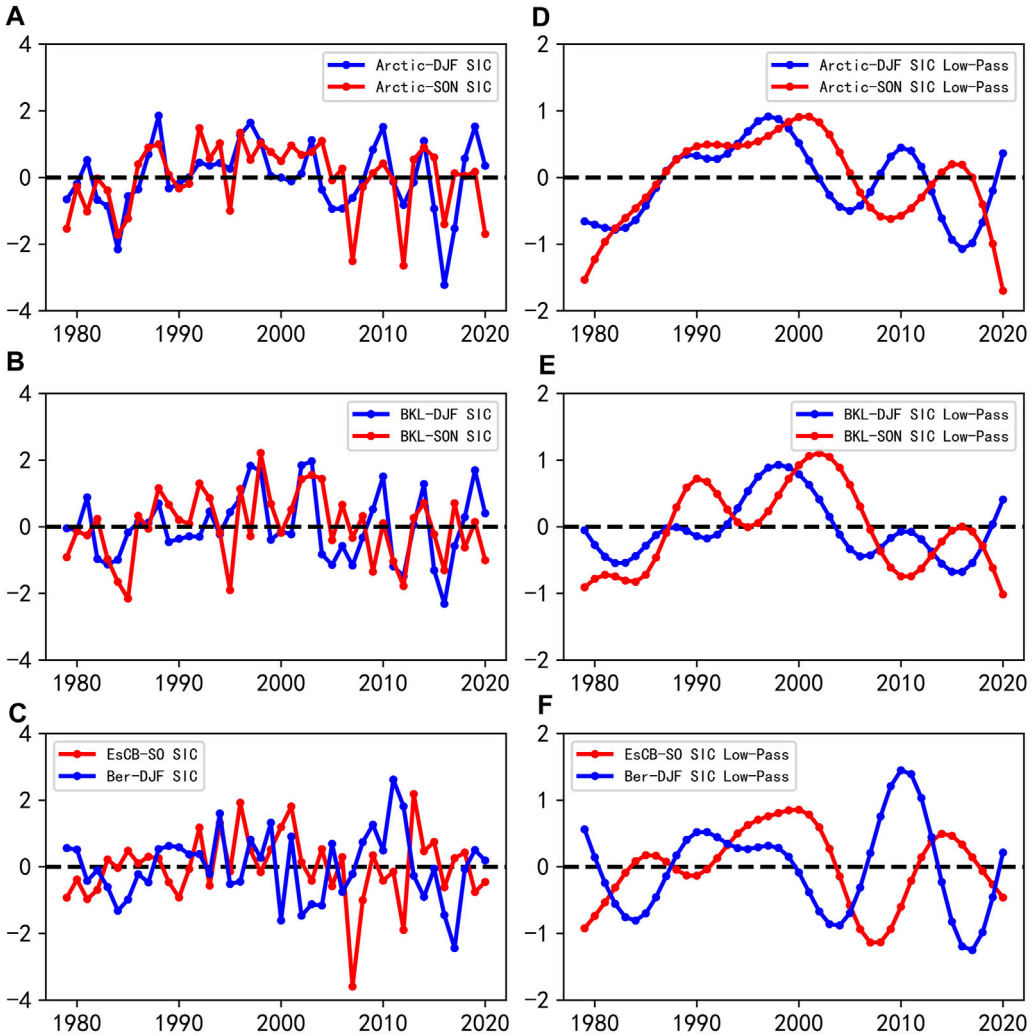

FIGURE 1 | Arctic sea-ice concentration (SIC) indices in different regions and seasons: **(A)** Pan-Arctic, **(B)** BKL in autumn (September–November) and winter (December–February), **(C)** EsCB in autumn (September–October) and Ber in winter. **(D–F)** As in **(A–C)** but for the corresponding 9-year low-pass filtered components. The blue (red) line denotes the winter (autumn) SIC index.

TABLE 1 | Explained variance of interannual and interdecadal components of raw SIC indices.

	Interannual (%)	Interdecadal (%)
Pan-arctic SON SIC	61.3	38.7
BKL SON SIC	61.8	38.2
EsCB SO SIC	68.0	32.0
Pan-Arctic DJF SIC	67.7	32.3
BKL DJF SIC	78.9	21.1
Ber DJF SIC	52.1	47.9

TABLE 2 | Correlation coefficients between Arctic SIC in diverse regions and seasons.

Pan-arctic SON SIC	Pan-arctic DJF SIC	0.51*
BKL SON SIC	BKL DJF SIC	042*
Ber SON SIC	Ber DJF SIC	0.37*
EsCB SO SIC	EsCB DJF SIC	0.26
Pan-Arctic SON SIC	BKL SON SIC	0.74*
Pan-Arctic SON SIC	EsCB SO SIC	0.70*
Pan-Arctic DJF SIC	BKL DJF SIC	0.83*
Pan-Arctic DJF SIC	Ber DJF SIC	0.30

Asterisk indicates correlation statistically significant at the 95% confidence level.

consistent in their amplitudes. Also of note is that the autumn EsCB and winter Ber are increasingly linked to the Pan-Arctic and BKL on interdecadal timescales since 2000, indicating that the interdecadal variation of Pan-Arctic sea-ice is mainly affected by sea-ice in the Atlantic sector and secondarily by sea-ice in the Pacific sector, while the contribution of Pacific sea-ice has increased since 2000. Considering the similarity in the SIC variation between the Pan-Arctic and BKL, their related atmospheric circulation and midlatitude climate anomalies should also resemble each other closely.

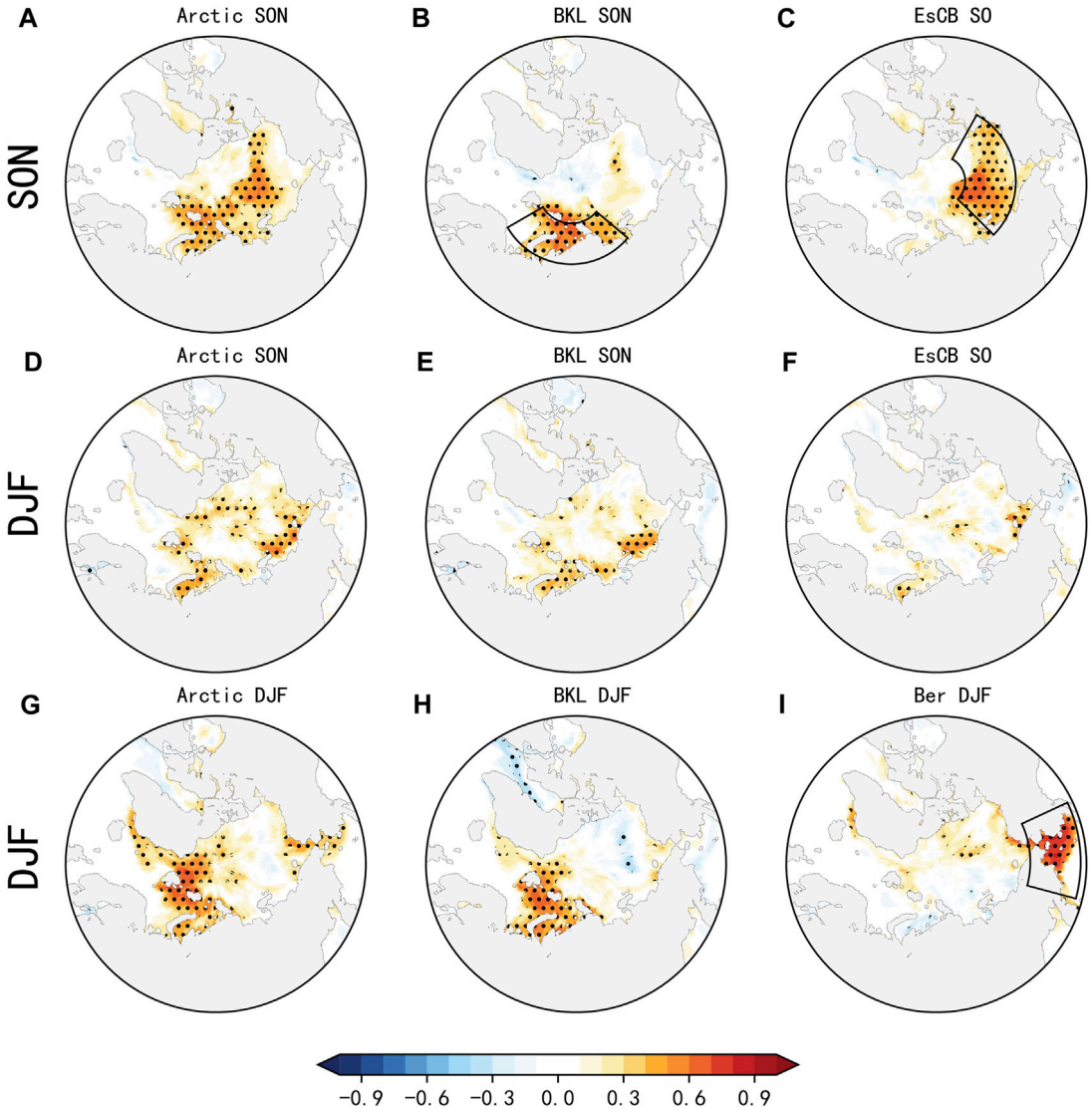

FIGURE 2 | Linear regression of **(A–C)** autumn and **(D–F)** winter Arctic SIC with respect to regional SIC indices in the Pan-Arctic, BKL and EsCB in autumn. **(G–I)** As in **(A–C)** but for winter SIC anomalies regressed upon winter indices. Rectangles denote the region to define BKL, EsCB, and Ber indices. Stippling indicates regression anomalies that are statistically significant at the 95% confidence level.

Autumn Sea-Ice–Related Temperature and Circulation

Previous studies have indicated that sea-ice loss coupled with cooling or a lack of warming in the midlatitudes causes the Arctic and midlatitude temperatures to diverge. The warm Arctic and cold continents/Eurasia (WACC/E) pattern constitutes the most robust observational evidence over the Northern Hemisphere midlatitudes in recent decades (Cohen et al., 2014; Cohen et al., 2020). However, the aforementioned studies focused mostly on year-round sea-ice change, with limited attention paid to autumn sea-ice change. **Figure 3** shows the wintertime SAT anomalies regressed upon the sea-ice indices in different regions. Consistent with previous studies, the autumn Pan-Arctic and BKL sea-ice loss have pronounced impacts on winter Eurasian coldness. There are also negative SAT anomalies over North America and positive ones over the Arctic Ocean, but the response is generally weaker and with patchy statistical significance (**Figures 3A,B**). The Northern Hemisphere midlatitude SAT anomalies are usually associated with large-scale atmospheric circulation changes. Eurasian cold anomalies are dynamically consistent with the negative phase of the NAO, enhanced and northward shifted Siberian high, and the Ural ridge of high pressure, featuring an equivalent barotropic structure (**Figures 4A,B**). These circulation changes imply meandering westerly winds, increased blocking frequency, and hence severe cold weather, which is consistent with the findings of previous studies, albeit

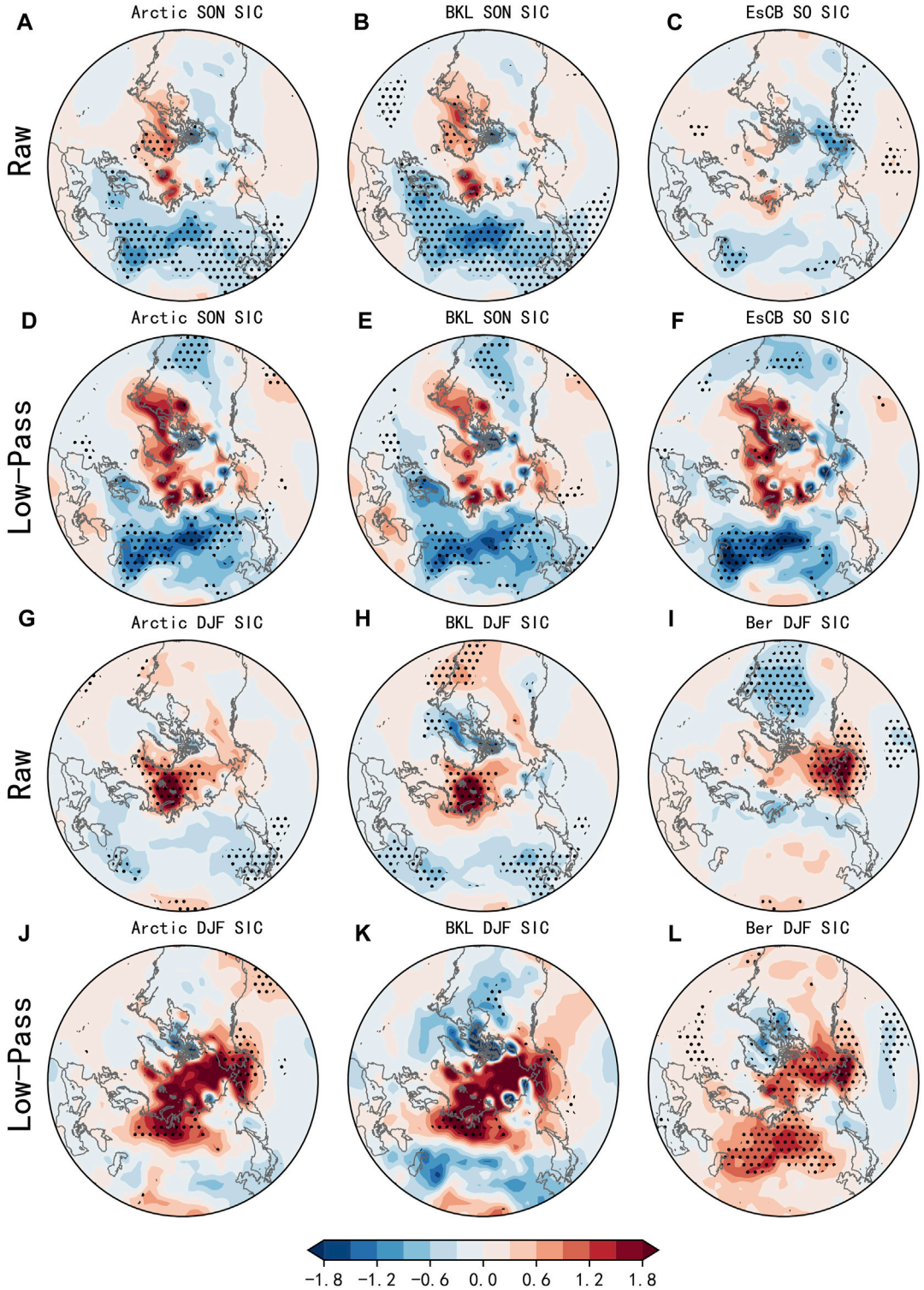

FIGURE 3 | Linear regression of winter surface air temperature (SAT; unit: K) anomalies against the Pan-Arctic, BKL and EsCB SIC indices **(A–C)** and associated interdecadal component **(D–F)** in autumn. **(G–L)** As in **(A–F)** but for SIC indices in winter. Stippling indicates SAT anomalies that are statistically significant at the 95% confidence level.

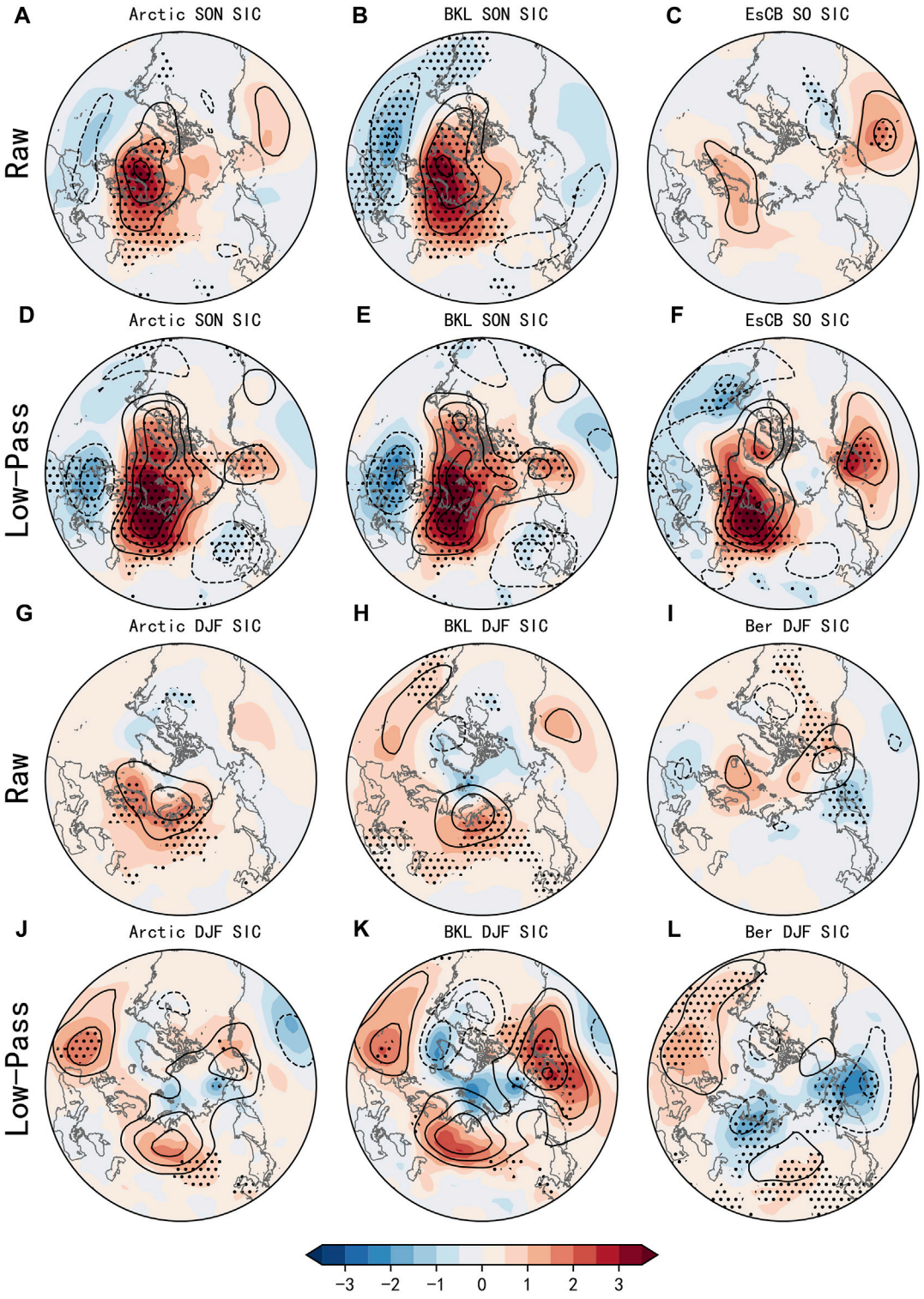

FIGURE 4 | As in **Figure 3** but for SLP (shading; unit: hPa) and 500-hPa geopotential height fields (contours; interval: 10 m).

that focused mainly on the effects of year-round or winter sea-ice loss (Mori et al., 2014; Ayarzagüena and Screen, 2016; Pedersen et al., 2016) rather than autumn sea-ice loss.

The mechanisms underpinning the influence of autumn sea-ice on the wintertime midlatitude climate are complex. Autumn sea-ice loss can modify large-scale Rossby waves by increasing the

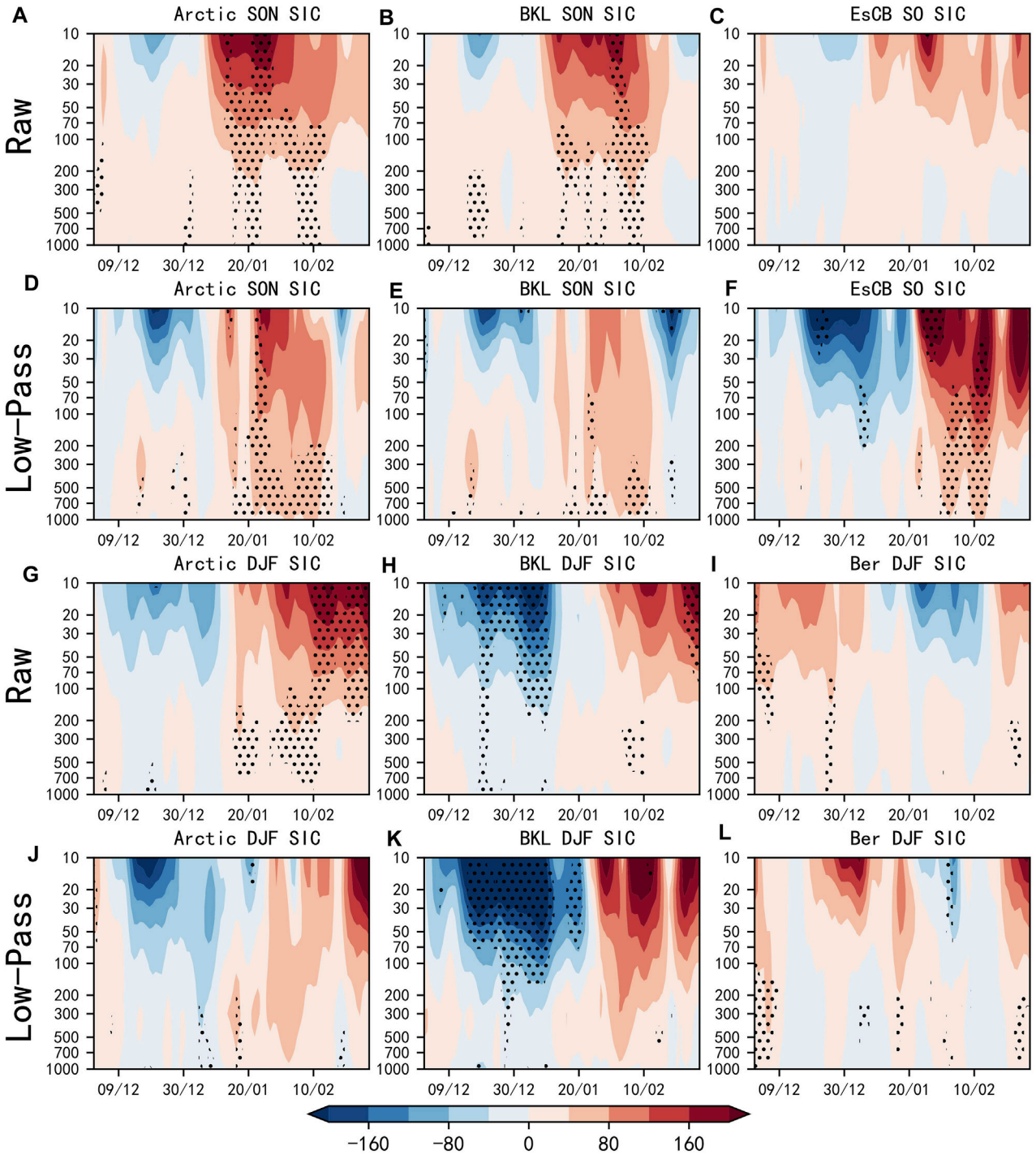

FIGURE 5 | As in **Figure 3** but for the winter daily evolution of polar cap height (PCH; 70°–90°N; unit: m).

vertical propagation of wave energy into the stratosphere, favoring a warmer and weakened stratospheric polar vortex. One common measure of such troposphere–stratosphere interaction is the evolution of polar cap height (PCH; e.g., Peings and Magnusdottir, 2014), which is calculated as the geopotential height averaged north of 70°N. **Figure 5** shows the winter PCH anomalies regressed upon the sea-ice indices in different regions and seasons. Autumn Pan-Arctic and BKL sea-ice loss favor significant positive PCH anomalies throughout the troposphere in winter, which increase in late December and January above 100 hPa, indicating a weakening of the polar vortex, consistent with Sun et al. (2015). Then, positive PCH

anomalies propagate downwards and reach the surface in mid-January and early February, leading to a negative phase of the NAO and hence significant cooling over large parts of Eurasia and North America (**Figures 5A,B**). This timing of the coldness is consistent with the findings of Peings and Magnusdottir (2014), who prescribed year-round sea-ice loss in an atmospheric model, indicating that the stratospheric pathway can be primarily attributed to sea-ice change in autumn.

A similar pattern of winter negative SAT anomalies over Eurasia is apparent for autumn EsCB, but the anomalies are relatively insignificant and spatially restricted when compared with the Pan-Arctic and BKL (**Figure 3C**). The positive PCH anomalies occur in the stratosphere but lack statistical significance, which implies the absence of stratospheric processes (**Figures 4C**, **5C**). Chen and Wu (2018) found significant stratospheric PCH responses over the mid–high latitudes in response to EsCB sea-ice loss in September–October on interannual timescales, but these PCH anomalies reach lower troposphere in March rather than in winter. Another significant cold SAT anomaly occurs over Alaska, and this coldness is associated with weakening of the Aleutian low possibly related to persistent EsCB sea-ice loss (**Figures 2C**, **3C**).

On the interdecadal timescale, autumn sea-ice loss in these subregions is connected with significant cooling over large parts of Eurasia and North America, and the correlations are statistically stronger than the unfiltered results (**Figures 3A–C**). This suggests that, in decadal periods of autumn sea-ice loss (gain), low (high) temperature anomalies are likely to occur over midlatitude land areas. In addition, it is interesting to note that lower-than-normal SAT anomalies are found over North America for all regional SIC indices and over the Eurasian midlatitudes for EsCB (**Figures 3D–F**), which disappear in the unfiltered results. This discrepancy implies that Arctic sea-ice loss has some physical linkage with North American coldness on interdecadal rather than interannual timescales, as well as the autumn EsCB-winter Eurasian SAT linkage. Reasons for this closer linkage are probably the stronger negative NAO phase and the enhanced Siberian high that stretch into North America (**Figures 4D–F**). Furthermore, the downward wave propagation to troposphere is significantly enhanced. In particular, the EsCB-related PCH anomalies display significant positive anomalies and propagate into the lower troposphere in early February (**Figures 5D–F**). These intensified circulation situations provide favorable conditions for the occurrence of cold temperatures in the Northern Hemisphere midlatitudes.

In conclusion, there is a dynamic relationship between autumn sea-ice loss in different regions and wintertime atmospheric circulation and attendant midlatitude coldness, mainly through stratospheric pathways. Specifically, the BKL sea-ice variation is closely related to the Eurasian midlatitude coldness on both interannual and interdecadal timescales, but to the North American coldness on the interdecadal timescale only. The EsCB sea-ice is connected with midlatitude coldness in Eurasia and North America on the interdecadal timescale.

Winter Sea Ice–Related Temperature and Circulation

Winter sea-ice has a different effect on wintertime atmospheric circulation relative to autumn sea-ice. As for winter Pan-Arctic and BKL sea-ice loss, cold anomalies in the Eurasian midlatitude are quite a lot weaker and lack statistical significance. Meanwhile, broad and significant Arctic warming is evident in regions of sea-ice loss (**Figures 3G,H**). Winter sea-ice loss corresponds to a weak positive phase of NAO pattern over the North Atlantic regions, which is different to the autumn sea-ice–related negative NAO pattern. The main positive anomaly centers are situated over Siberia and the North Atlantic, with the Siberian high relatively weaker in magnitude and more zonally orientated when compared with autumn sea-ice-related circulation anomalies (**Figures 4G,H**). That is the reason why low temperatures occur over Northeast China along the eastern margin of the high pressure. In cases of BKL sea-ice loss, the expansion of Davis Strait sea-ice is conducive to the anomalous low pressure over Greenland-northern North America and the anomalous high pressure over North Atlantic (Dai et al., 2019). In addition, the weak positive NAO pattern is very likely attributed to the strengthened and significant stratospheric polar vortex in early winter (**Figures 5G,H**). The stratospheric process associated with winter sea-ice loss differs from that with autumn sea-ice loss. In late winter, the stratospheric process is characterized by a weakened polar vortex, weak downward propagation in late January and obvious upward propagation of tropospheric waves in February. This weak stratospheric process related with winter sea-ice loss is different from the robust stratospheric process in Zhang et al. (2018), since their focus is sea-ice loss in November–December, while our focus is December–February. These results suggest that the tropospheric pathway may play a major role in the impacts of winter sea-ice change on Eurasian climate, while stratospheric pathway play a minor role.

In comparison, the winter Ber is linked to significant cooling over eastern North America and evident warming over the Aleutian region of sea-ice loss (**Figure 3I**), consistent with previous results (Kug et al., 2015; Screen, 2017A). In the troposphere, there is a clear wave train downstream of the Bering Sea, dynamically connected with an anomalous high over Alaska, which plays a vital role in linking the reduction in Ber sea-ice to the cold conditions in eastern North America (**Figure 4I**). This result is in agreement with Iida et al. (2020) that winter Bering sea-ice loss can affect wintertime North American cold anomalies by changing the Alaska Oscillation, the dominant mode over the highlatitude North Pacific. In the stratosphere, there is insignificant downward propagation of the positive PCH response that emerges in late December and early February (**Figure 5I**). Likewise, the stratospheric pathway is less important in the linkage between the winter Ber and the cold conditions in North American.

On the interdecadal timescale, the Eurasian midlatitude cold temperature is statistically insignificant; and furthermore, in turn, overall warming is apparent over the Arctic with penetration into northern Eurasia. Conversely, the North

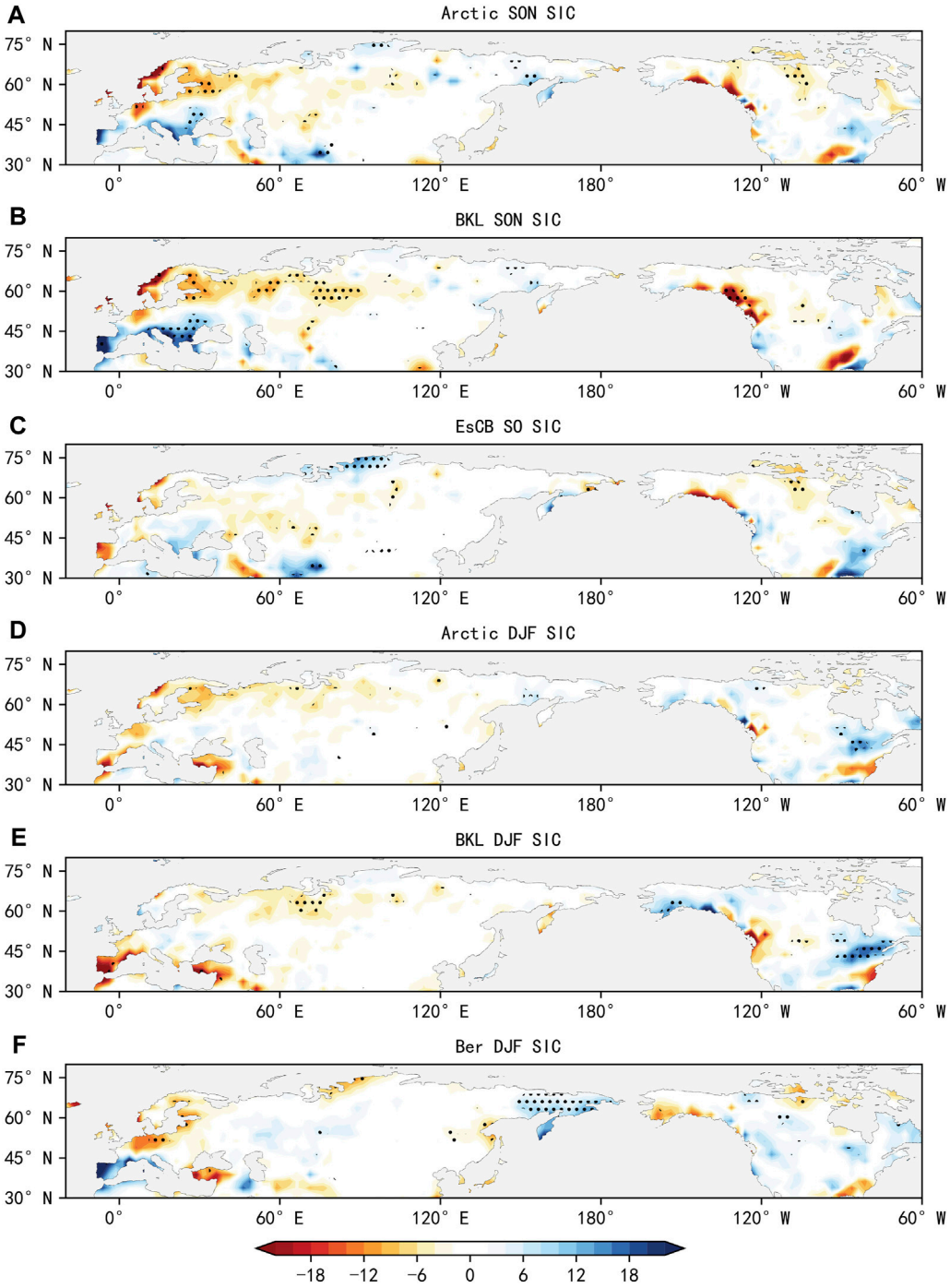

FIGURE 6 | As **Figures 3A–C** and **Figures 3G–I** but for monthly mean precipitation over land (unit: mm).

American midlatitude cold temperature is robust (**Figures 3J,K**). This indicates that in decades with Pan-Arctic and BKL sea-ice loss (gain) in winter, the highlatitude Eurasia tend to be warmer (colder) and the midlatitude Eurasian cold conditions tend to be milder (warmer) and the midlatitude North America tend to be colder (warmer), contrary to autumn sea-ice loss. The Siberian high shifts southwards in position and the positive NAO pattern is more apparent when compared with that associated with autumn sea-ice change (**Figures 4J,K**). The southerly winds along the western margin of the Siberian high guide warm air to the Arctic and Eurasian highlatitude regions; and meanwhile, warm advection along the eastern margin transports warm air from the open oceans to the Eurasian highlatitudes, leading to the

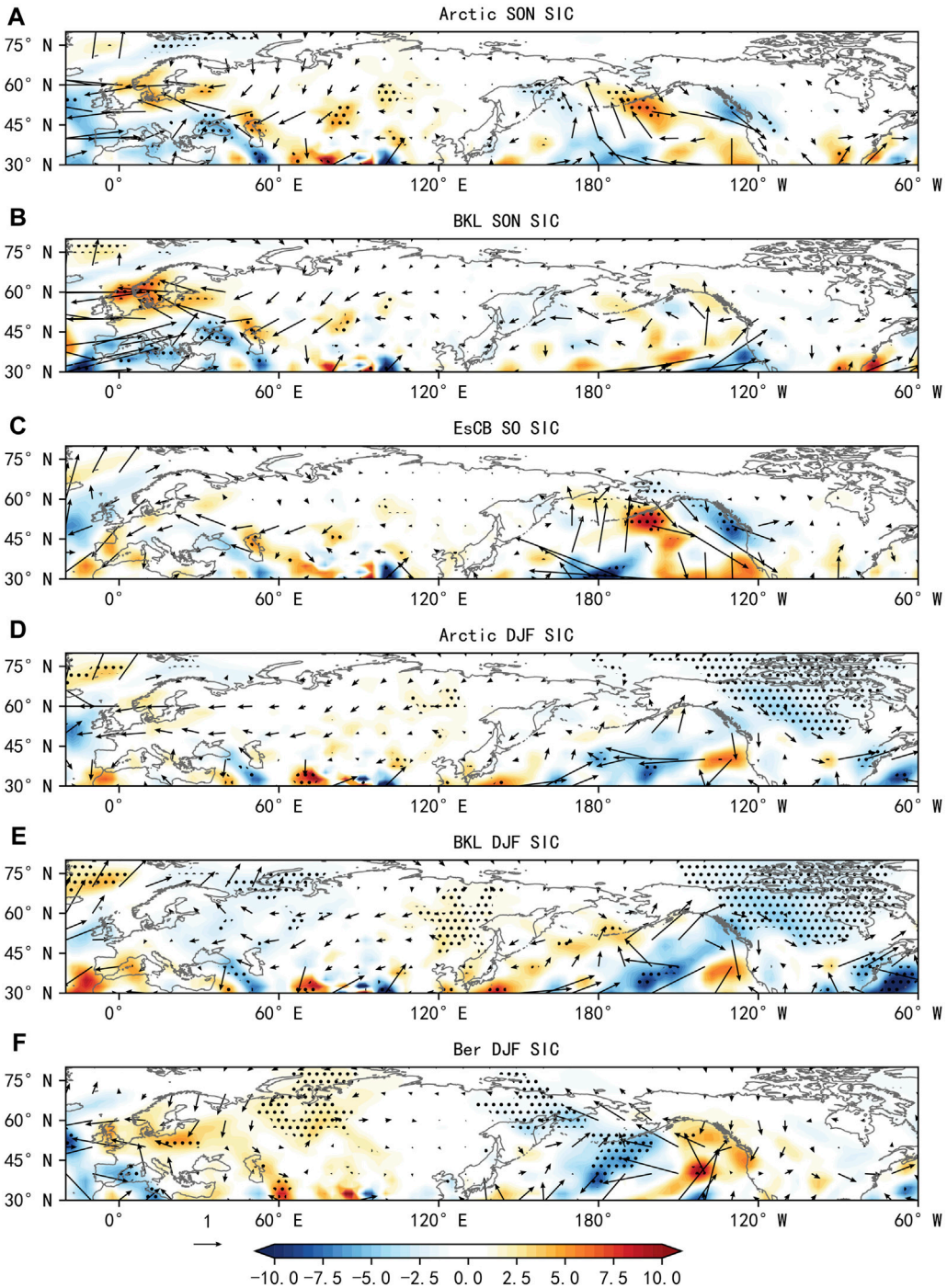

FIGURE 7 | As in **Figure 6** but for 1,000–500-hPa cumulative moisture transport fluxes [vectors; units: g (m s)$^{-1}$] and associated divergence [shading; units: g (m^2 s)$^{-1}$].

warm highlatitude Eurasia. Furthermore, significantly negative PCH anomalies are overwhelmingly found throughout the troposphere and stratosphere, leading to the positive NAO pattern and cold North America. Therefore, it can be concluded that the Eurasian highlatitude warming and weakened midlatitude cooling is dynamically linked to winter sea-ice loss in BKL, mainly through tropospheric rather than stratospheric pathways.

As for Ber, there is significant SAT warming in central Eurasia and Alaska and insignificant warming over North America (**Figure 3L**). The latter warming is contrary to the unfiltered cooling over North America, indicating that the impacts of Ber

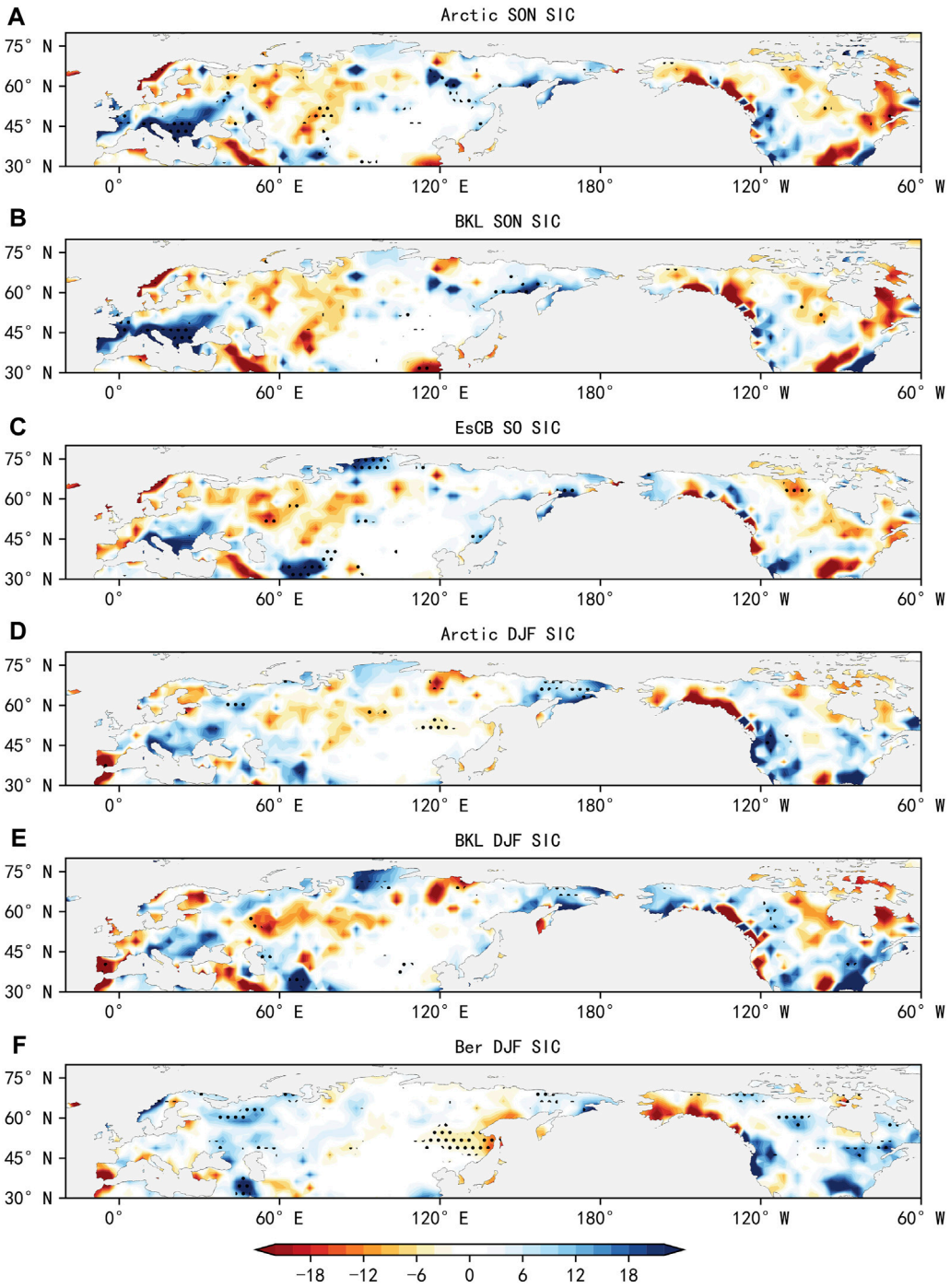

FIGURE 8 | As in **Figure 6** but for the interdecadal component of precipitation.

sea-ice on North American cooling possibly exist at the interannual timescale (figure not shown) rather than the interdecadal timescale. A circumglobal-scale teleconnection wave train, with high pressure anomalies over East Asia, a strengthened Aleutian low, and weakened high-pressure anomalies over Alaska (**Figure 4L**), is favorable for the occurrence of warm temperatures over central Eurasia. In addition, the low pressure in the Aleutian region is contrary to autumn sea-ice-induced high anomalies, which implies that atmospheric circulation dominates the Bering Sea and that the southerly winds guide warm air northwards to the Bering Sea and hence ice loss happens there. The stratospheric pathway, however, has little impact on the wintertime climate (**Figure 5L**).

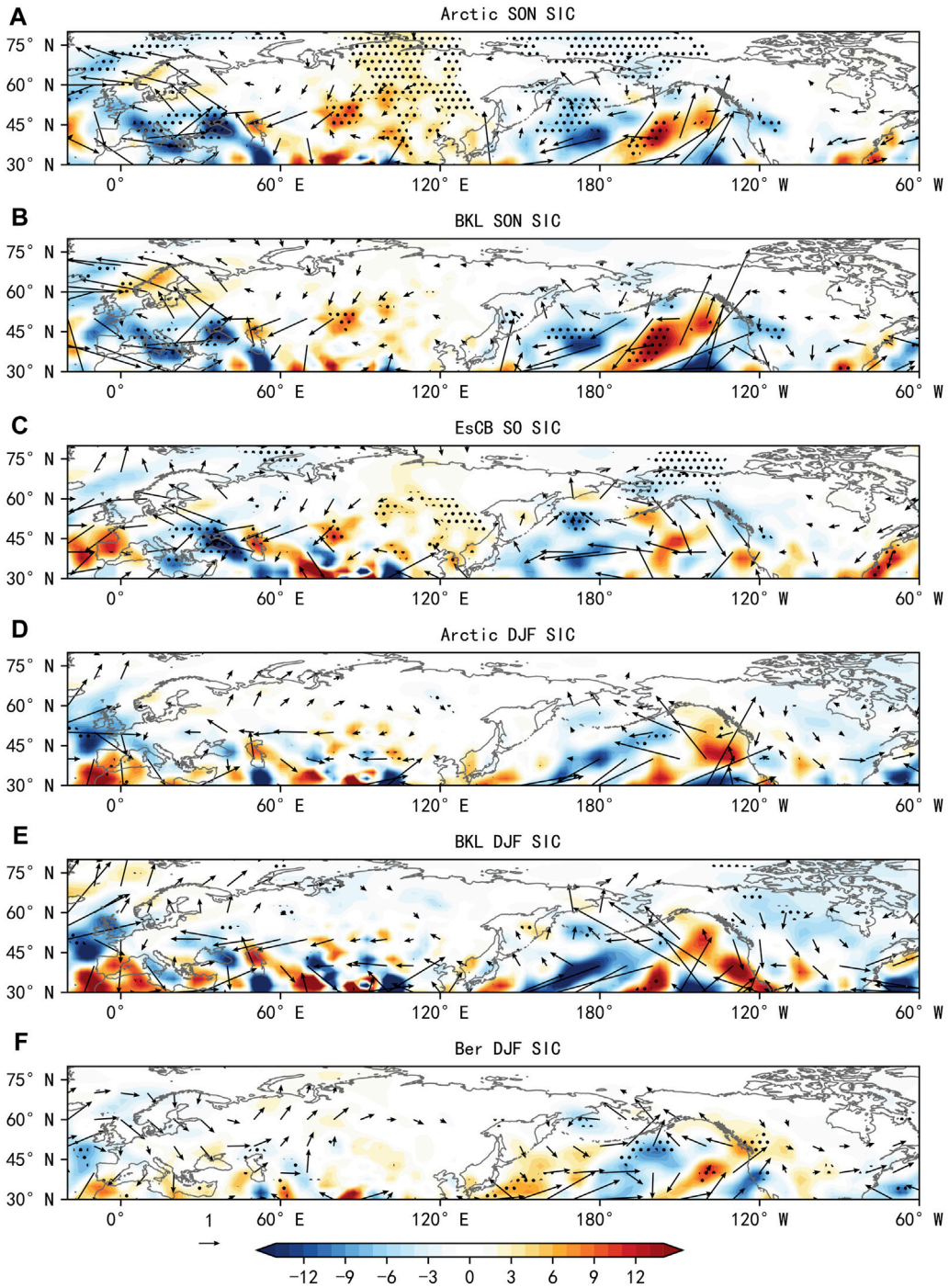

FIGURE 9 | As in **Figure 7** but for the interdecadal component of moisture transport fluxes and associated divergence.

Generally speaking, the winter BKL sea-ice loss (gain) is linked to an enhanced (a weakened) Siberian high and lower (higher) temperatures in the highlatitudes of Eurasia. In contrast, the winter sea-ice loss (gain) in Ber is linked to a large-scale teleconnection wave train downstream of the Bering Sea, with higher (lower) than normal temperature in North America on the interannual timescale and in central Eurasia on the interdecadal timescale.

Precipitation and Moisture Transport

In addition to temperature, large-scale circulation anomalies associated with Arctic sea-ice variation also affect precipitation. On the one hand, strengthening of the Siberian high caused by melting of Arctic sea-ice changes the precipitation pattern in the midlatitudes (Gong and Ho, 2002). On the other hand, the expansion of the Arctic open

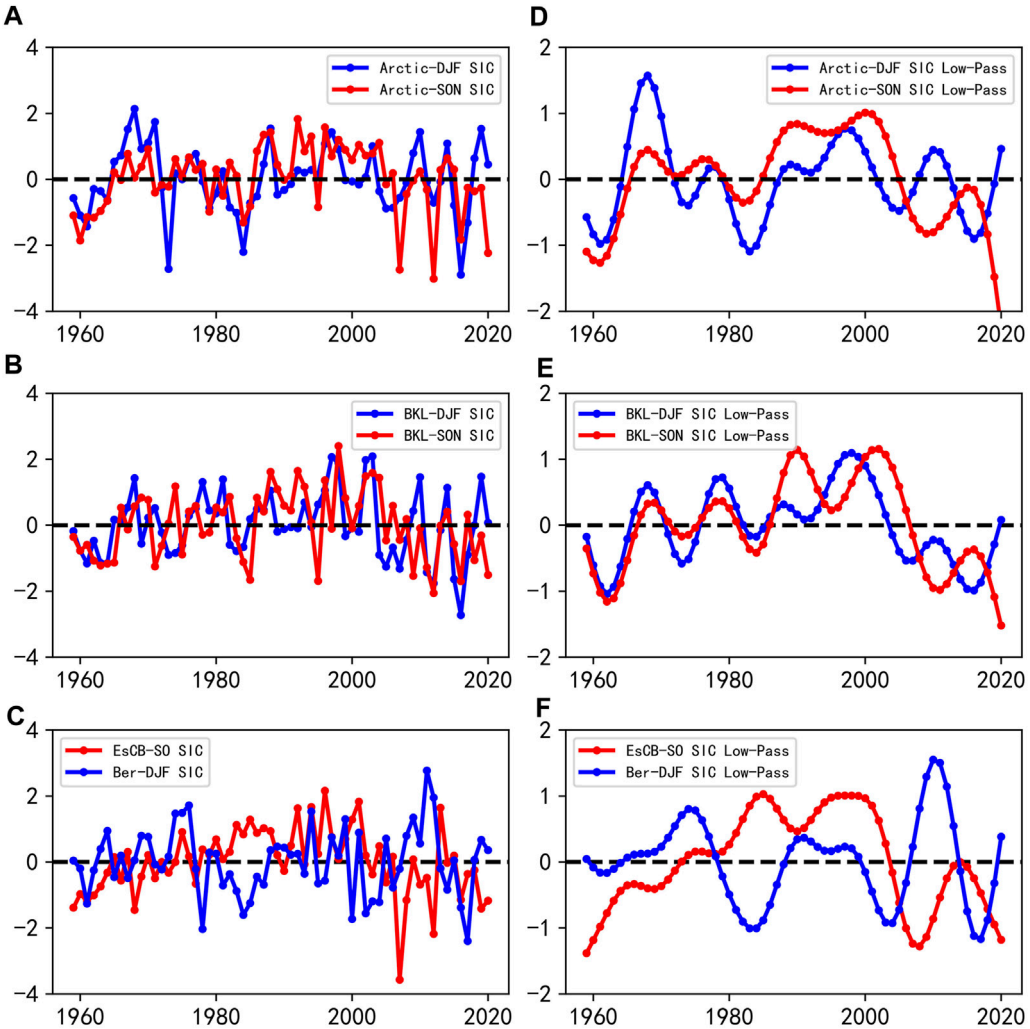

FIGURE 10 | As in **Figure 1** but for the period from 1959 to 2020.

ocean also provides water vapor conditions for precipitation over the continent (Ben et al., 2016). **Figures 6–9** show the wintertime precipitation and large-scale moisture flux anomalies regressed upon the sea-ice in different regions and seasons.

In terms of autumn Pan-Arctic and BKL sea-ice loss, a meridional dipole precipitation anomaly pattern can be found in the Northern Hemisphere mid–high-latitudes, which shows more precipitation over the midlatitudes, such as in southern Europe, and little precipitation at highlatitudes, such as northwestern Eurasia and northeastern Canada (**Figures 6A,B**). This dipole pattern is mainly affected by the anomalous anticyclone over Siberia and the Canadian Archipelago, which gives rise to apparent water vapor divergence over Eurasian highlatitudes and northeastern Canada, leading to a deficit in precipitation over these regions. Meanwhile, the anomalous anticyclone over the North Atlantic–Europe region converges water vapor flux from the Atlantic and Eurasia (**Figures 7A,B**), resulting in increased precipitation over southern Europe. This wintertime precipitation pattern is similar to that in Li and Wang (2012), who applied the autumn Kara–Laptev sea-ice index during 1982–2010 for regression. For EsCB, due to the weak circulation anomalies, water vapor flux and precipitation anomalies are broadly weak (**Figures 6C**, **7C**).

On the interdecadal timescale, the precipitation anomalies related to autumn sea-ice loss in the three regions show similar dipole patterns, but with stronger precipitation in magnitude and a southward extension of the deficit in precipitation in central Eurasia. This dipole pattern is due to the meridional enhancement and expansion of Siberia–North America high pressure anomalies, which facilitate an increased frequency of cold and dry air into Siberia and North America. Meanwhile, the negative precipitation anomalies over northeast Canada are spreading towards southeast Canada. Moreover, the anomalous cyclone located in the northeast Atlantic–Europe region is strengthened, relative to the unfiltered results, and facilitates water vapor transport from the Atlantic and

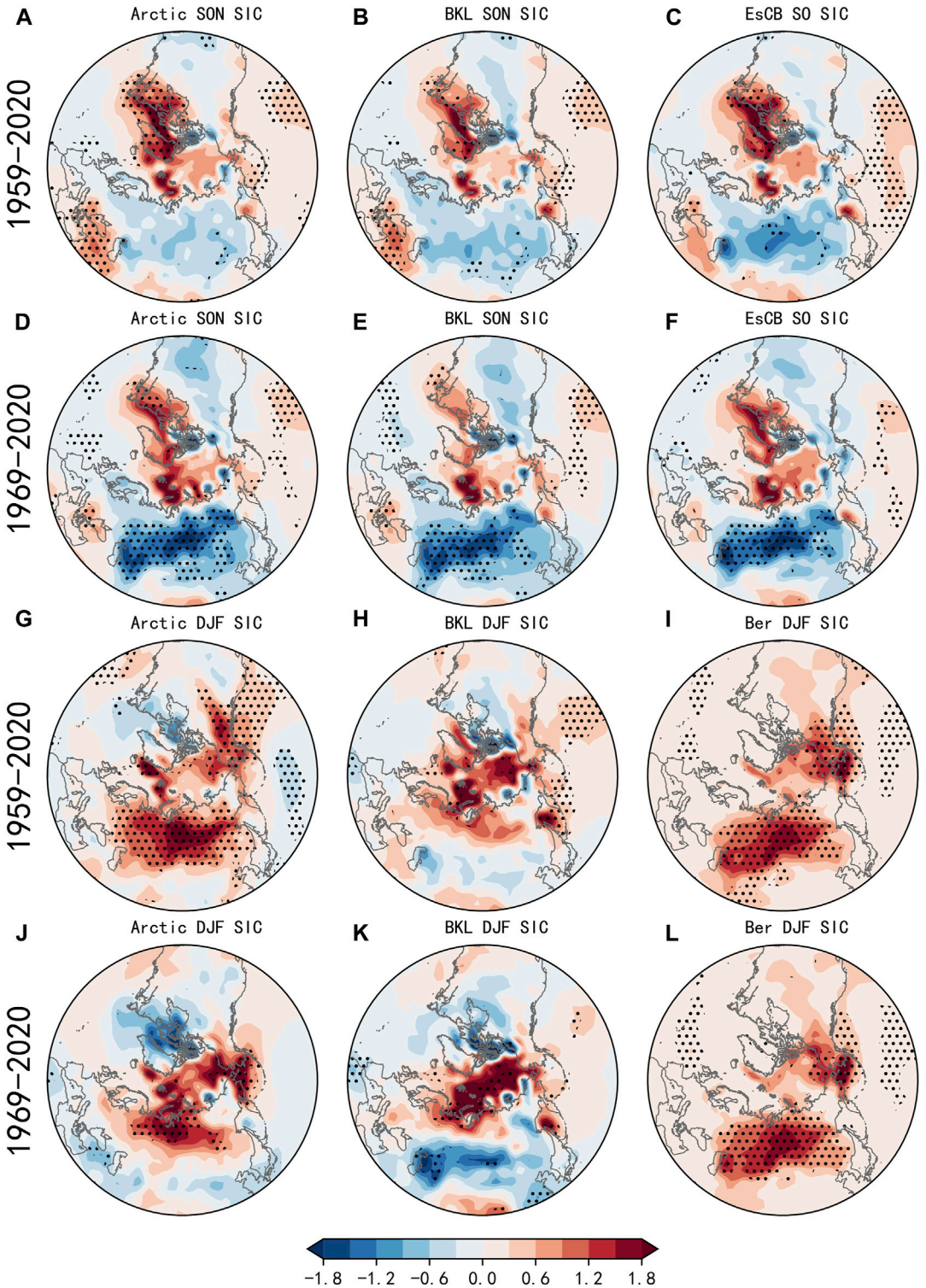

FIGURE 11 | As in **Figure 3** but for interdecadal component of sea-ice indices and surface air temperature during 1959–2020 [**(A–C)** and **(G–I)**] and 1969–2020 [**(D–F)** and **(J–L)**].

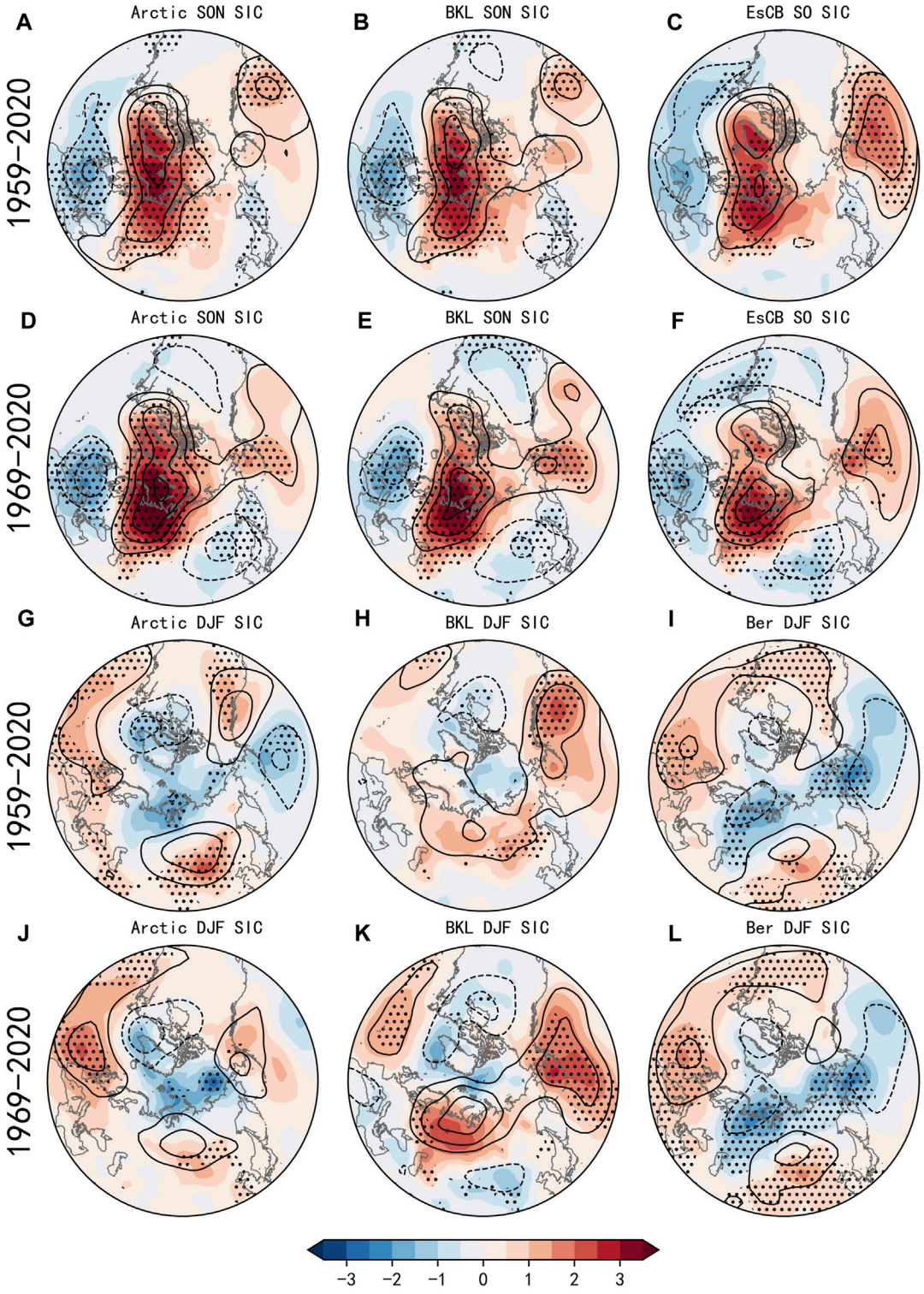

FIGURE 12 | As in **Figure 4** but for interdecadal sea-ice loss during 1959–2020 [**(A–C)** and **(G–L)**] and 1969–2020 [**(D–F)** and **(J–L)**].

Mediterranean (**Figures 8A–C**; **Figures9A–C**). Therefore, the dipole pattern is strengthened in intensity, and the area influenced is enlarged to nearby regions.

For the winter Pan-Arctic and BKL sea-ice loss, insufficient precipitation is generally observed in Eurasia, which corresponds to the more extensive Siberian high and accompanies a divergence

in moisture transport. The anomalous low pressure in northern North America is favorable for the convergence of water vapor and excessive precipitation over the northeastern United States (**Figures 6D,E**; **Figures 7D,E**). For the winter Ber, the moisture flux and precipitation anomalies over both continents are weak. However, the Alaskan high pressure and melting Ber sea-ice facilitate water vapor convergence in the Far East, contributing to increased precipitation there (**Figures 6F**, **7F**).

On the interdecadal timescale, the main difference for the Pan-Arctic and BKL is the north–south tripole pattern of precipitation over the Eurasian continent, with high snowfall around the Arctic and in southern Europe and low snowfall in the midlatitudes. This is because the anomalous Siberian high moves southwards, which leads to the southward displacement of the dipole pattern identified in the unfiltered results. In addition, the high snowfall around the Arctic can be attributed to the increased area of open water, and the Siberian high transports more water vapor from BKL to the Eurasian highlatitudes. However, the cause of the increase in precipitation over southern Europe is different to that in the unfiltered results **Figures 3A-C**. The high pressure anomaly over western Europe and the westerly winds carry water vapor from the North Atlantic to southern Europe. In North America, the low pressure over northeastern North America and the high pressure over the Aleutian region appear to guide water vapor from the Arctic *via* the northerly winds, resulting in more precipitation over northwestern and southeastern North America (**Figures 8D,E**; **Figures 9D,E**). For the Bering Sea, due to the anticyclonic circulation near the Barents Sea, the water vapor from the Arctic Ocean and Europe converges in eastern Europe, leading to abundant precipitation there. Northeast China is located at the eastern margin of the anomalous Eurasian high, which is controlled by the dry current from the northern continent and hence dominated by reduced precipitation. Similar to the Pan-Arctic and BKL, the low pressure over northern North America and the high pressure over the northern Atlantic facilitate water vapor convergence in northern and central North America, with moisture sources from the Arctic, North America and North Atlantic (**Figures 8F**, **9F**).

To conclude, changes in precipitation are dynamically consistent with large-scale atmospheric circulation and temperature. The precipitation patterns associated with autumn sea-ice change on interdecadal timescales resemble those in the unfiltered results, which display a north–south dipole pattern over the Northern Hemisphere. For winter sea-ice change, a north–south tripole pattern is identifiable for BKL, and excessive European precipitation is apparent for Ber.

CONCLUSION AND DISCUSSION

The interdecadal linkage between the wintertime Northern Hemisphere climate and sea-ice in different regions and seasons is analyzed in this paper. The results can be summarized as follows:

The Pan-Arctic and BKL sea-ice, irrespective of seasonality, display similar relationships with large-scale atmospheric circulation, near-surface air temperature, and precipitation anomalies. The WACC mode of wintertime temperature is dynamically consistent with the sea-ice loss in both autumn and winter. Autumn sea-ice loss can affect the wintertime climate in the midlatitudes through stratospheric pathways, which generally leads to a negative NAO phase with an anomalous high over the Arctic and continental highlatitudes. These anomalous circulations appear to induce severe cold events in the midlatitudes, albeit still controversially, and a north–south dipole precipitation pattern over Northern Hemisphere continents. However, wintertime sea-ice loss affects the climate mainly through tropospheric pathways. Significant warming is observed over the Arctic and extends to highlatitudes, whereas mild coldness is found in the midlatitudes. For precipitation, there is a meridional "less-more-less" tripole pattern over the Eurasian continent and abundant precipitation over North America.

The atmospheric circulation and climate anomalies associated with autumn EsCB shows similarity to those with Pan-Arctic and BKL on the interdecadal timescale, but large difference on the interannual timescale. For winter, however, the Ber-related circulation and climate anomalies differ from those of the Pan-Arctic and BKL. There are low pressure centers over Siberia and northeastern North America and hence positive precipitation anomalies there, and high pressure over East Asia and hence strong central Eurasian warming.

The present study focuses on the interdecadal relationship between the Arctic and midlatitudes during the 1979–2020 period. Given that the periodism of Arctic sea-ice indices is shorter than 20 years, it appears reasonable to conduct interdecadal analysis using 40-year dataset. To further verify the interdecadal variations of sea-ice on longer timescale, we extend the period of dataset to 1959 and 1969, respectively. **Figures 10–12** show the Arctic sea-ice indices and associated SAT, and SLP and 500-hPa geopotential height anomalies. Prior to 1979, there is relatively heavy than average sea-ice in diverse regions, and high persistence of sea-ice anomalies between autumn and winter (**Figure 10**). The temperature and circulation anomalies during the 1969–2020 and 1979–2020 periods are similar in spatial pattern and magnitude, particularly for the robust Eurasian cooling (**Figure 11**). The main difference is the disappearance of significant cold anomalies over North America, which is caused by the stronger low pressure anomalies over North America (**Figure 12**). For the 1959–2020 period, the spatial patterns remain similar, but the magnitudes largely reduce and lack statistical significance. This is because the NAO pattern and Siberian high are relatively weaker, in companion with the weakened East Asian trough, which is conducive to cold-air outbreaks into the midlatitudes (**Figure 12**). Another reason for the differences between different periods, is the lack of sea-ice data until the satellite era. Before sea-ice can be seen from satellites, rather coarse indicators of the sea-ice have been monitored and higher spatial resolution sea-ice data can be acquired for recent three decades (Rayner et al., 2003; Coon et al., 2007).

Another question worthy of discussion is the nonstationary relationship betweensea-ice and wintertime climate in long-term timescales. In this study, comparing dataset of long period to short period, this interdecadal linkage begins to attenuate and lacks statistical significance. For the 1850–2099 period, Kolstad and Screen (2019) discovered evidence of nonstationarity in the relationship between autumn sea-ice and the winter NAO, which implicates that the recently intimate ice-NAO relationship is unstable. Furthermore, recent studies reported that weakened positive anomaly of Siberian High after the mid-1990s is induced by lesser Kara-Laptev sea-ice loss, and that enhanced spring AO after the late-1990s is caused by larger interannual variability of Laptev-eastern Siberian-Beaufort sea ice (Chen et al., 2019; 2020B). These results implicate that the circulation anomalies caused by sea-ice change are strongly dependent upon the analysis period and the location of sea-ice loss.

These findings have important implications for seasonal and interdecadal forecasting in the future, especially in the context of ongoing sea-ice loss. However, some regional precipitation anomalies still cannot be explained by mid–high-latitude circulation anomalies; for example, the precipitation anomalies over southeastern North America where there are complex tropical-extratropical interactions. Previous studies have also demonstrated that precipitation inland is strongly influenced by climate change (Lin and Zhou, 2015; Zhao et al., 2019) and El Niño–Southern Oscillation (ENSO) (Zhou and Wu, 2010), amongst other factors. Furthermore, recent studies have indicated that wintertime Arctic sea-ice anomalies can also have a significant impact on tropical climate systems, including the ENSO and Intertropical Convergence Zone, through large-scale atmospheric wave trains and equatorial warm Kelvin wave and monotonic temperature increase in deep ocean, respectively. (e.g., Wang et al., 2018; Chen et al., 2020A). Therefore, sensitivity experiments are needed to isolate the individual effect of Arctic sea-ice. Furthermore, it is important to note that statistical association does not guarantee causality. As such, to further demonstrate the part of the midlatitude climate anomalies caused by sea-ice change in distinct geographical regions and seasons, coupled model simulations are required, which is the next step for our group's research (Kim et al., 2014; Screen, 2017a).

DATA AVAILABILITY STATEMENT

The original contributions presented in the study are included in the article/Supplementary Material, further inquiries can be directed to the corresponding author.

AUTHOR CONTRIBUTIONS

XH and RZ conceived the study and wrote the manuscript. SD and ZZ provided critical feedback and helped shape the research and manuscript. All authors contributed to the article and approved the submitted version.

FUNDING

RZ was supported by the National Key Research and Development Program of China (Grants 2016YFA0601500 and 2019YFC1509105), National Natural Science Foundation of China (Grants 41790472 and 42075016), and Shanghai Pujiang Program (Grant 2020PJD004).

REFERENCES

Ayarzagüena, B., and Screen, J. A. (2016). Future Arctic Sea Ice Loss Reduces Severity of Cold Air Outbreaks in Midlatitudes. *Geophys. Res. Lett.* 43, 2801–2809. doi:10.1002/2016GL068092

Ben, G. K., Kopec, X., Michel, F. A., and Posmentier, E. S. (2016). Influence of Sea Ice on Arctic Precipitation. *Proc. Natl. Acad. Sci. U S A.* 113, 46–51. doi:10.1073/pnas.1504633113

Chen, S., Wu, R., and Chen, W. (2019). Enhanced Impact of Arctic Sea Ice Change during Boreal Autumn on the Following spring Arctic Oscillation since the Mid-1990s. *Clim. Dyn.* 53, 5607–5621. doi:10.1007/s00382-019-04886-y

Chen, S., and Wu, R. (2018). Impacts of Early Autumn Arctic Sea Ice Concentration on Subsequent spring Eurasian Surface Air Temperature Variations. *Clim. Dyn.* 51, 2523–2542. doi:10.1007/s00382-017-4026-x

Chen, S., Wu, R., Chen, W., and Yu, B. (2020a). Influence of winter Arctic Sea Ice Concentration Change on the El Niño-Southern Oscillation in the Following winter. *Clim. Dyn.* 54, 741–757. doi:10.1007/s00382-019-05027-1

Chen, S., Wu, R., Cheng, W., and Yu, B. (2020b). Weakened Impact of Autumn Arctic Sea Ice Concentration Change on the Subsequent winter Siberian High Variation Around the Late-1990s. *Int. J. Climatol* 41, 2700–2717. doi:10.1002/joc.6875

Cohen, J., Screen, J. A., Furtado, J. C., Barlow, M., Whittleston, D., Coumou, D., et al. (2014). Recent Arctic Amplification and Extreme Mid-latitude Weather. *Nat. Geosci* 7, 627–637. doi:10.1038/ngeo2234

Cohen, J., Zhang, X., and Francis, J. (2020). Divergent Consensuses on Arctic Amplification Influence on Midlatitude Severe winter Weather. *Nat. Clim. Chang* 10, 20–29. doi:10.1038/s41558-019-0662-y

Coon, M., Kwok, R., Levy, G., Pruis, M., Schreyer, H., and Sulsky, D. (2007). Arctic Ice Dynamics Joint Experiment (AIDJEX) Assumptions Revisited and Found Inadequate. *J. Geophys. Res.* 112 (C11), C11S90. doi:10.1029/2005JC003393

Dai, H., Fan, K., and Liu, J. (2019). Month-to-Month Variability of Winter Temperature over Northeast China Linked to Sea Ice over the Davis Strait-Baffin Bay and the Barents-Kara Sea. *J. Clim.* 32, 6365–6384. doi:10.1175/JCLI-D-18-0804.1

Davis, R. (1976). Predictability of Sea Surface Temperature and Sea Level Pressure Anomalies over the North Pacific Ocean. *J. Phys. Oceanography* 6, 249–266. doi:10.1175/1520-0485(1976)006,0249:POSSTA.2.0.CO;2

Ding, S., Wu, B., and Chen, W. (2020). Dominant Characteristics of Early Autumn Arctic Sea Ice Variability and its Impact on Winter Eurasian Climate. *J. Clim.* 34 (5), 1–67.

Ding, S., and Wu, B. (2021). Linkage between Autumn Sea Ice Loss and Ensuing spring Eurasian Temperature. *Clim. Dyn*. doi:10.1007/s00382-021-05839-0

Francis, J. A., and Vavrus, S. J. (2012). Evidence Linking Arctic Amplification to Extreme Weather in Mid-latitudes. *Geophys. Res. Lett.* 39, a–n. doi:10.1029/2012GL051000

Gong, D.-Y., and Ho, C.-H. (2002). The Siberian High and Climate Change over Middle to High Latitude Asia. *Theor. Appl. Climatology* 72, 1–9. doi:10.1007/s007040200008

Honda, M., Inoue, J., and Yamane, S. (2009). Influence of Low Arctic Sea-ice Minima on Anomalously Cold Eurasian winters. *Geophys. Res. Lett.* 36, L08707. doi:10.1029/2008GL037079

Iida, M., Sugimoto, S., and Suga, T. (2020). Severe Cold Winter in North America Linked to Bering Sea Ice Loss. *J. Clim.* 33, 8069–8085. doi:10.1175/JCLI-D-19-0994.1

Kalnay, E., Kanamitsu, M., Kistler, R., Collins, W., Deaven, D., Gandin, L., et al. (1996). The NCEP/NCAR 40-year Reanalysis Project. *Bull. Amer. Meteorol. Soc.* 77, 437–470.

Kim, B.-M., Son, S.-W., Min, S.-K., Jeong, J.-H., Kim, S.-J., Zhang, X., et al. (2014). Weakening of the Stratospheric Polar Vortex by Arctic Sea-Ice Loss. *Nat. Commun.* 5, 4646. doi:10.1038/ncomms5646

Kolstad, E. W., and Screen, J. A. (2019). Nonstationary Relationship between Autumn Arctic Sea Ice and the winter North Atlantic Oscillation. *Geophys. Res. Lett.* 46, 7583–7591. doi:10.1029/2019GL083059

Kug, J.-S., Jeong, J.-H., Jang, Y.-S. Min., Kim, B.-M., Folland, C. K., Min, S.-K., et al. (2015). Two Distinct Influences of Arctic Warming on Cold winters over North America and East Asia. *Nat. Geosci* 8, 759–762. doi:10.1038/NGEO2517

Li, C., Stevens, B., and Marotzke, J. (2015). Eurasian winter Cooling in the Warming Hiatus of 1998-2012. *Geophys. Res. Lett.* 42, 8131–8139. doi:10.1002/2015GL065327

Li, F., and Wang, H. (2012). Autumn Sea Ice Cover, Winter Northern Hemisphere Annular Mode, and Winter Precipitation in Eurasia. *J. Clim.* 26, 3968–3981. doi:10.1175/JCLI-D-12-00380.1

Lin, R., and Zhou, T. (2015). Reproducibility and Future Projections of the Precipitation Structure in East Asia in Four Chinese GCMs that Participated in the CMIP5 Experiments. *Chin. J. Atmos. Sci.* 39, 338–356. doi:10.3878/j.issn.1006-9895.1407.14110

Liu, N., Lin, L., Kong, B., Wang, Y., Zhang, Z., and Chen, H. (2016). Association between Arctic Autumn Sea Ice Concentration and Early winter Precipitation in China. *Acta Oceanol. Sin.* 35, 73–78. doi:10.1007/s13131-016-0860-7

Ma, J., Wang, H., and Zhang, Y. (2012). Will Boreal winter Precipitation over China Increase in the Future? an AGCM Simulation under Summer "Ice-free Arctic" Conditions. *Chin. Sci. Bull.* 57, 921–926. doi:10.1007/s11434-011-4925-x

Mori, M., Kosaka, Y., Watanabe, M., Nakamura, H., and Kimoto, M. (2019). A Reconciled Estimate of the Influence of Arctic Sea-Ice Loss on Recent Eurasian Cooling. *Nat. Clim Change* 9, 123–129. doi:10.1038/s41558-018-0379-3

Mori, M. M., Shiogama, H., Inoue, J., and Kimoto, M. (2014). Robust Arctic Sea-Ice Influence on the Frequent Eurasian Cold winters in Past Decades. *Nat. Geosci* 7, 869–873. doi:10.1038/NGEO2277

Nakamura, T., Yamazaki, K., Iwamoto, K., Honda, M., Miyoshi, Y., Ogawa, Y., et al. (2016). The Stratospheric Pathway for Arctic Impacts on Midlatitude Climate. *Geophys. Res. Lett.* 43, 3494–3501. doi:10.1002/2016GL068330

Nakamura, T., Yamazaki, K., Iwamoto, K., Honda, M., Miyoshi, Y., and Ukita, J. (2014). A Negative Phase Shift of the winter AO/NAO Due to the Recent Arctic Sea-Ice Reduction in Late Autumn. *J. Geophys. Res. Atmos.* 120, 3209–3227. doi:10.1002/2014JD022848

Pedersen, R. A., Cvijanovic, I., Langen, P. L., and Vinther, B. M. (2016). The Impact of Regional Arctic Sea Ice Loss on Atmospheric Circulation and the NAO. *J. Clim.* 29, 889–902. doi:10.1175/JCLI-D-15-0315.1

Peings, Y., and Magnusdottir, G. (2014). Response of the Wintertime Northern Hemisphere Atmospheric Circulation to Current and Projected Arctic Sea Ice Decline: A Numerical Study with CAM5. *J. Clim.* 27, 244–264. doi:10.1175/JCLI-D-13-00272.1

Peings, Y., and Magnusdottir, Y. G. (2015). Role of Sea Surface Temperature, Arctic Sea Ice and Siberian Snow in Forcing the Atmospheric Circulation in winter of 2012-2013. *Clim. Dyn.* 45, 1181–1206. doi:10.1007/s00382-014-2368-1

Rayner, N. A., Parker, D. E., Horton, E. B., and Folland, A. (2003). Global Analyses of Sea Surface Temperature, Sea Ice, and Night marine Air Temperature since the Late Nineteenth century. *J. Geophys. Res.* 108, 4407. doi:10.1029/2002JD002670

Screen, J. A. (2017a). Far-flung Effects of Arctic Warming. *Nat. Geosci* 10, 253–254. doi:10.1038/ngeo2924

Screen, J. A. (2017b). Simulated Atmospheric Response to Regional and Pan-Arctic Sea Ice Loss. *J. Clim.* 30, 3945–3962. doi:10.1175/JCLI-D-16-0197.1

Selesnick, I. W., and Burrus, C. S. (1998). Generalized Digital Butterworth Filter Design. *IEEE Trans. Signal. Process.* 46 (6), 1688–1694. doi:10.1109/78.678493

Song, L., Wang, L., Chen, W., and Zhang, Y. (2016). Intraseasonal Variation of the Strength of the East Asian Trough and its Climatic Impacts in Boreal winter. *J. Clim.* 29, 2557–2577. doi:10.1175/JCLI-D-14-00834.1

Sun, J., and Wang, H. (2012). Changes of the Connection between the Summer North Atlantic Oscillation and the East Asian Summer Rainfall. *J. Geophys. Res.* 117, a–n. doi:10.1029/2012JD017482

Sun, L., Deser, C., and Tomas, R. A. (2015). Mechanisms of Stratospheric and Tropospheric Circulation Response to Projected Arctic Sea Ice Loss*. *J. Clim.* 28, 7824–7845. doi:10.1175/JCLI-D-15-0169.1

Sun, L., Perlwitz, J., and Hoerling, M. (2016). What Caused the Recent "Warm Arctic, Cold Continents" Trend Pattern in winter Temperatures?. *Geophys. Res. Lett.* 43, 5345–5352. doi:10.1002/2016gl069024

Takaya, K., and Nakamura, H. (2005). Mechanisms of Intraseasonal Amplification of the Cold Siberian High. *J. Atmos. Sci.* 62, 4423–4440. doi:10.1175/JAS3629.1

Trenberth, K. E. (1999). Atmospheric Moisture Recycling: Role of Advection and Local Evaporation. *J. Clim.* 12, 1368–1381. doi:10.1175/1520-0442(1999)012<1368:AMRROA>2.0.CO;2

Van Oldenborgh, G. J., Haarsma, R., De Vries, H., and Allen, M. R. (2015). Cold Extremes in North America vs. Mild Weather in Europe: The Winter of 2013-14 in the Context of a Warming World. *Bull. Amer. Meteorol. Soc.* 96, 707–714. doi:10.1175/BAMS-D-14-00036.1

Wang, K., Deser, C., Sun, L., and Tomas, R. A. (2018). Fast Response of the Tropics to an Abrupt Loss of Arctic Sea Ice *via* Ocean Dynamics. *Geophys. Res. Lett.* 45, 4264–4272. doi:10.1029/2018GL077325

Wang, S., Nath, D., and Chen, W. (2021). Nonstationary Relationship between Sea Ice over Kara–Laptev Seas during August–September and Ural Blocking in the Following winter. *Int. J. Climatol.* 41 (Suppl. 1), E1608–E1622. doi:10.1002/joc.6794E1622

WMO Regional Climate Centres (2012). *Cold Spell in Europe and Asia in Late winter 2011/2012. Issued by WMO Regional Climate Centres: RA II (Asia): Tokyo Climate Centre, Japan Meteorological Agency (JMA). RA VI (Europe): Pilot Regional Climate Centre, node on Climate Monitoring (RCC-CM), Lead Centre Deutscher Wetterdienst (DWD), Germany*. WMO Regional Climate Centres, 20. available at: http://reliefweb.int/sites/reliefweb.int/files/resources/dwd_2012- _report.pdf.

Wu, B., Su, J., and Zhang, R. (2011). Effects of Autumn-winter Arctic Sea Ice on winter Siberian High. *Chin. Sci. Bull.* 56, 3220–3228. doi:10.1007/s11434-011-4696-4

Wu, B., Yang, K., and Francis, J. A. (2017). A Cold Event in Asia during January-February 2012 and its Possible Association with Arctic Sea Ice Loss. *J. Clim.* 30, 7971–7990. doi:10.1175/JCLI-D-16-0115.1

Xie, P., and Arkin, P. A. (1997). Global Precipitation: A 17-year Monthly Analysis Based on Gauge Observations, Satellite Estimates, and Numerical Model Outputs. *Bull. Amer. Meteorol. Soc.* 78, 2539–2558. doi:10.1175/1520-0477(1997)078<2539:GPAYMA>2.0.CO;2

Zhang, P., Wu, Y., Simpson, I. R., Smith, K. L., Zhang, X., De, B., et al. (2018). A Stratospheric Pathway Linking a Colder Siberia to Barents-Kara Sea Sea Ice Loss. *Sci. Adv.* 4, eaat6025. doi:10.1126/sciadv.aat6025

Zhang, R. N., and Screen, J. A. (2021). Diverse Eurasian winter Temperature Responses to Barents-Kara Sea Ice Anomalies of Different Magnitudes and Seasonality. *Geophys. Res. Lett.* 48, e2021GL092726. doi:10.1029/2021gl092726

Zhang, R., Zhang, R., and Dai, G. (2021). Intraseasonal Contributions of Arctic Sea-Ice Loss and Pacific Decadal Oscillation to a century Cold Event during Early 2020/21 winter. *Clim. Dyn.*. doi:10.1007/s00382-021-05931-5

Zhao, Y., Xiao, D., and Pai, H. (2019). Projection and Application for Future Climate in china by CMIP5 Climate Model. *Meteorol. Sci. Technol.* 47, 608–621. doi:10.1002/joc.5409

Zhou, L.-T., and Wu, R. (2010). Respective Impacts of the East Asian winter Monsoon and ENSO on winter Rainfall in China. *J. Geophys. Res.* 115, D02107. doi:10.1029/2009JD012502

Conflict of Interest: The authors declare that the research was conducted in the absence of any commercial or financial relationships that could be construed as a potential conflict of interest.

Publisher's Note: All claims expressed in this article are solely those of the authors and do not necessarily represent those of their affiliated organizations, or those of the publisher, the editors and the reviewers. Any product that may be evaluated in this article, or claim that may be made by its manufacturer, is not guaranteed or endorsed by the publisher.